

Subcritical instability of Taylor–Couette flow with stationary inner cylinder

J. M. Lopez

School of Mathematical and Statistical Sciences, Arizona State University, Tempe, AZ 85287, USA

Abstract

The presence of endwalls in Taylor–Couette flows has far reaching effects, leading to dynamics that are qualitatively different to the idealized flow involving infinitely long cylinders. This is well known when the inner cylinder is rotating and the outer cylinder is stationary. The effects of endwalls in the centrifugally stable situation with stationary inner cylinder have not been previously considered in detail. The meridional flows induced by the endwalls lead to the formation of a thin sidewall boundary layer on the inner cylinder wall if the endwalls are rotating, or on the outer cylinder wall if they are stationary. At sufficiently high Reynolds numbers, the sidewall boundary layer has concentrated shear, the pressure gradient in the azimuthal direction (which is the streamwise direction for the boundary layer flow) is zero (the flow is axisymmetric) and the boundary layer thickness is constant. At a critical Reynolds number, the sidewall boundary layer loses stability at a subcritical Hopf bifurcation, breaking the axisymmetry of the flow, and for Reynolds numbers slightly above critical, a packet of Hopf modes with azimuthal wavenumbers clustered about the critical wavenumber grow. The early time evolution of the critical Hopf mode is a rotating wave analogous to a Tollmien–Schlichting wave. As the Hopf modes grow, nonlinear interactions lead to modulations, localization of the disturbances and the evolution of concentrated streamwise vortical streaks which become very long and intense via vortex stretching.

Introduction

Circular Couette flow is the flow in the annular gap between two rotating cylinders. Recently, there has been much interest in regimes where linear stability theory for the infinite length annulus predicts the flow to be stable to centrifugal instability, as it may be nonlinearly unstable [3]. For the infinite length annulus, the basic state is steady, axisymmetric and axially invariant, and its azimuthal velocity has a well-known analytic form, given by $v(r) = ar + b/r$, where the constants a and b are determined by the radii of the inner and outer cylinders and their angular speeds [6]. With the inner cylinder stationary and the outer cylinder rotating, this flow is linearly stable.

The linear stability of the finite case has not been previously analyzed. Recent experiments utilizing both visualization and velocimetry report subcritical transition to turbulence for Reynolds numbers of order 10^5 in the wide gap regime, as well as a considerable hysteresis range in Reynolds number between the laminar and turbulent states [2]. Computing the basic states at these high Reynolds numbers is not trivial due to the thin boundary layers involved. Furthermore, obtaining the basic state experimentally at the high Reynolds number end of the hysteresis region is very challenging due to noise and imperfections triggering transition to turbulence [1].

Here, the axisymmetric basic state is computed for Reynolds numbers a little beyond 10^5 , and stability to general three-dimensional perturbations is determined via temporal evolution of the three-dimensional Navier–Stokes equations. It is shown that there is a critical Reynolds number, which depends on the annulus geometry and whether the endwalls are stationary or

rotating with the outer cylinder, beyond which the basic state is unstable. The very early time evolution of the perturbations for Reynolds numbers beyond critical show exponential growth, the perturbation flow has a moderate azimuthal wavenumber, and is localized in the sidewall boundary layer of the inner cylinder if the endwalls are rotating or in the outer cylinder boundary layer if the endwalls are stationary. The basic state is unstable to a band of azimuthal wavenumbers, centered about the critical wavenumber. As the perturbation grows and nonlinear effects become important, modulations caused by the sideband modes lead to one of the azimuthal cells growing faster than the others, and its broad cellular structure becomes concentrated into a pair of vortical streaks aligned with the mean flow direction in the boundary layer either side of the mid-height of the annulus. The streaks become elongated in the azimuthal direction, with the local vorticity and local velocity becoming more aligned. Vortex stretching leads to their rapid intensification, to the point where the numerics are unable to resolve them. This development has much in common with the shear instability of zero-pressure gradient boundary layers, where Tollmien–Schlichting waves first grow exponentially, become unstable to a modulation, followed by a rapid transition to turbulence [5].

Governing equations and numerical technique

Consider the flow in an annulus of height H , inner radius R_i , and outer radius R_o , completely filled with a fluid of kinematic viscosity ν . The flow is driven by the constant rotation of the outer cylinder at angular speed Ω and the inner cylinder is kept stationary. We consider two cases, one where the top and bottom endwalls are rotating with the outer cylinder, and the other where the endwalls are stationary.

The annular gap, $D = (R_o - R_i)$, is used as the length scale, and the viscous time across the gap, D^2/ν , is used for the time scale. The flow is governed by three parameters: Reynolds number $Re = \Omega R_o D/\nu$, aspect ratio H/D , and radius ratio R_i/R_o . The non-dimensional Navier–Stokes equations are:

$$(\partial_t + \mathbf{u} \cdot \nabla) \mathbf{u} = -\nabla p + \nabla^2 \mathbf{u}, \quad \nabla \cdot \mathbf{u} = 0, \quad (1)$$

where p is the pressure and $\mathbf{u} = (u, v, w)$ is the velocity field which we will represent in cylindrical coordinates (r, θ, z) , with $r \in [r_i = R_i/R_o/(1 - R_i/R_o), r_o = 1/(1 - R_i/R_o)]$, $\theta \in [0, 2\pi)$ and $z \in [-0.5H/D, 0.5H/D]$. The vorticity field is $\nabla \times \mathbf{u} = (\xi, \eta, \zeta)$ and the helicity is $He = \mathbf{u} \cdot (\nabla \times \mathbf{u})$. The boundary conditions on the inner and outer cylinder are:

$$\mathbf{u}(r_i, \theta, z) = (0, 0, 0) \quad \text{and} \quad \mathbf{u}(r_o, \theta, z) = (0, Re, 0), \quad (2)$$

and on the endwalls, the two cases are:

$$\text{stationary:} \quad \mathbf{u}(r, \theta, \pm 0.5H/D) = (0, 0, 0), \quad (3)$$

$$\text{rotating:} \quad \mathbf{u}(r, \theta, \pm 0.5H/D) = (0, (1 - R_i/R_o)rRe, 0). \quad (4)$$

The Navier–Stokes equations are solved using a second-order time-splitting method with consistent boundary conditions for the pressure. Spatial discretization is via a Galerkin–Fourier expansion in θ and Chebyshev collocation in r and z . For the results presented here, we have fixed $H/D = 1$ and $R_i/R_o = 0.5$ and have considered Re up to 5×10^5 .

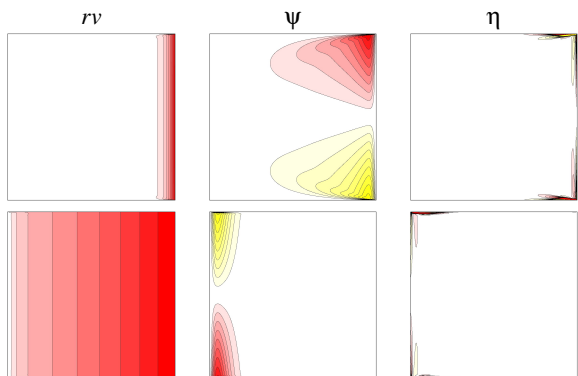


Figure 1: Vortex lines, streamlines, and azimuthal vorticity of the basic states at $Re = 10^5$ with stationary endwalls (top row) and rotating endwalls (bottom row).

The basic states have been computed using $n_r = n_z = 160$ Chebyshev modes in the radial and axial directions. In determining stability to three-dimensional perturbations, up to $n_\theta = 64$ has been used. The stability of the basic states was determined via time evolution; using the basic state at a given point in parameter space, a small (of order 10^{-8}) random perturbation was introduced at all (r, z) collocation points for the azimuthal Fourier wavenumber $m = 1$, and this is propagated to all azimuthal wavenumbers via the nonlinear terms. After some time, either all perturbations decay towards machine zero, indicating that the basic state at that point in parameter space is stable, or the perturbations organize themselves and have positive exponential growth, much as in a generalized power method. The growing perturbation does not need to nonlinearly saturate in order to determine its growth rate, and so the method is efficient in determining the growth rate and structure of the corresponding eigenmode. This is aided by monitoring the modal kinetic energies

$$E_m = 0.5 \int_0^{2\pi} \int_{-0.5H/D}^{0.5H/D} \int_{r_i}^{r_o} \mathbf{u}_m \mathbf{u}_m^* r dr dz d\theta, \quad (5)$$

where \mathbf{u}_m is the m th azimuthal Fourier mode of the velocity field and \mathbf{u}_m^* is its complex conjugate.

Results

Figure 1 shows the vortex lines (isocontours of rv), streamlines, and isocontours of azimuthal vorticity η , for basic states at $Re = 10^5$. For the stationary endwalls case, the vortex lines all enter and leave the annulus at the small gaps in the corners where the rotating outer sidewall and the stationary endwalls meet. Since the vortex lines are tangential to the stationary endwalls, there is vortex line bending producing azimuthal vorticity, which in turn results in large-scale meridional circulations that are clockwise in the bottom half and counter-clockwise in the top half. The meridional circulations tend to further advect the vortex lines radially inwards along the two endwalls, and the return flow is radially outwards along the mid-height, leading to an intense boundary layer on the outer cylinder. When the endwalls are co-rotating with the outer cylinder, most of the vortex lines originate at the bottom endwall and terminate at the top endwall and the flow in the bulk away from the inner cylinder boundary layer region is in solid-body rotation. Again, the fact that some vortex lines need to meet at the corners leads to vortex line bending that drives a meridional flow radially outward along the endwalls and radially inward along the mid-height. Intense boundary layers are established along the endwalls and on the inner cylinder. Further details on the structure of the boundary layers are available [4].

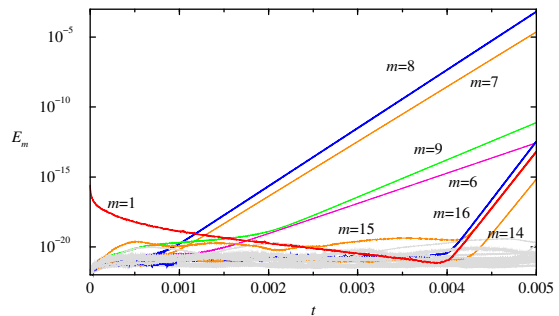


Figure 2: Time series of E_m , showing $m \geq 1$ (E_0 remains of order 10^{11}). The initial condition consists of the basic state at $Re = 2.6 \times 10^5$ with rotating endwalls, to which a random perturbation was introduced into azimuthal Fourier mode $m = 1$.

Figure 2 shows an example of the temporal evolution of the modal kinetic energies following a perturbation to a basic state. Specifically, it corresponds to taking as the initial condition the basic state at $Re = 2.6 \times 10^5$ with rotating endwalls, and at $t = 0$ random perturbations of order 10^{-8} are applied to the $m = 1$ Fourier component of the velocity. The corresponding modal energy of the perturbation is $E_1 \sim 10^{-16}$. This is a very small perturbation; the basic state has all of its kinetic energy in the axisymmetric component of the velocity and $E_0 \sim Re^2$. The nonlinear terms in the Navier–Stokes equations propagate the small perturbations to all azimuthal wavenumbers. The initial evolution of this nonlinear initial value problem is analogous to performing a matrix-free generalized power method, where the actions of the Jacobian matrices for the perturbations are given by the time integration of the Navier–Stokes equations. If the basic state is unstable to any non-axisymmetric mode, time evolution organizes the flow into these modes, and if the basic state is unstable to more than one mode, these unstable modes initially evolve independently because nonlinear couplings between them are at levels below numerical round-off noise and are hence negligible. The system, especially at high Re , is non-normal and so transient growth is also possible. In the nonlinear initial value problem, both linear non-normal transients and linearly unstable eigenmodes compete. The unstable modes grow exponentially, quickly overtaking any algebraic transient growth activity.

Figure 2 shows that following the initial impulse, E_1 decays to machine noise levels, but that by $t \approx 0.001$, the flow has organized itself and E_8 begins to grow exponentially, and very shortly after E_7 also begins to grow at a slightly slower rate. At $t \approx 0.0015$, E_9 and E_6 are also growing, but with much slower rates. These discrete azimuthal wavenumbers constitute a band of modes to which the basic state is unstable, and while their magnitudes remain small, they are evolving independently of one another. Their independent evolution is verified by the fact that E_1 is decaying while all four of these modes are growing. By $t \approx 0.004$, $E_8 \sim 10^{-7}$ and now the $m = 8$ mode is large enough that nonlinearities are no longer negligible. This is seen in the growth of its first harmonic, E_{16} . Also, there is now nonlinear interaction between $m = 8$ and $m = 7$ leading to growth in E_1 . The nonlinear interactions between $m = 8$, $m = 7$ and $m = 1$ result in growths of $m = 14$ and $m = 15$ as well. Note however that E_9 and E_6 are still several orders of magnitude smaller than E_8 and E_7 at this time, and continue to grow independently of everything else that is happening.

The structure of the flow perturbation consists of eight pairs of rolls that extend from endwall to endwall within the thin inner cylinder boundary layer, with little distortion in their shape but attaining maximum strength near the mid-height. These are

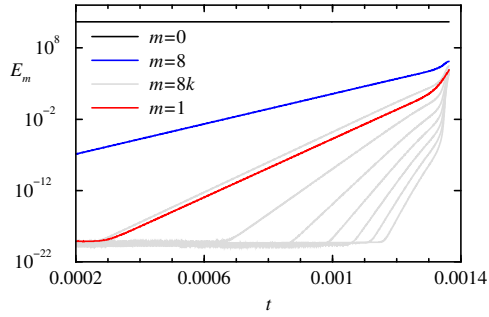


Figure 3: Time series of modal kinetic energies, E_0, E_1, E_8 and the harmonics E_{8k} for $k \in [2, 8]$ (the other E_m are not shown for clarity of presentation), for the rotating endwalls case at $Re = 4 \times 10^5$. The initial condition consisted of the axisymmetric basic state to which a small random perturbation in the Fourier mode $m = 1$ was introduced at $t = 0$, giving an initial $E_1 \sim 10^{-23}$. Shown is the evolution of E_m from $t = 0.0002$, just before the first harmonic E_{16} begins to grow, following which E_1 begins to grow, leading to the localization of the disturbance.

analogous to Tollmien–Schlichting waves. The axial and azimuthal vorticity components are confined very deep inside the boundary layer, and while they consist of eight pairs of structures of alternating sign as well, these structures are stretched out in the azimuthal direction by the mean azimuthal velocity in the boundary layer. The perturbation does not consist of eight identical pairs of structures; modulations from the other azimuthal wavenumbers that are shown in figure 2 are evident.

Evolutions of the type described above have been computed for many Re , for both the rotating and the stationary endwalls cases. The two endwall cases are similar in many respects. In both cases, the sidewall boundary layer thickness is less than 5% of the annular gap, and the azimuthal wavelength is the same for both. Note that the circumference of the outer cylinder is twice that of the inner cylinder, and the most amplified azimuthal wavenumber for the stationary endwalls case is $m = 16$ and for the rotating endwalls case it is $m = 8$. In the rotating endwalls case, the inner cylinder boundary layer has an outer flow that is nominally solid-body rotation and the boundary (inner cylinder) is stationary. For the stationary endwalls cases, the boundary layer is on the rotating outer cylinder and the outer flow is nominally stationary. Viewing this from a frame of reference rotating with the outer cylinder brings this case in line with the rotating endwalls cases, except that for the boundary layer flow on the inner cylinder, the curvature is convex and for the boundary layer flow on the outer cylinder the curvature of concave. However, the thinness of the boundary layers suggests that curvature effects are negligible, and the difference in the sign of curvature does not result in any qualitative differences in the two flow cases.

The band of Hopf modes with azimuthal wavenumbers centered about the critical wavenumber lead to nonlinear modulation as the perturbations grow and nonlinear interactions. If the bifurcations were supercritical, then one of the perturbation modes would saturate nonlinearly at the expense of the others and a new stable solution with the winning m would appear (which m wins depends on initial conditions), and this new state would be a rotating wave since the rotational invariance of the system is broken at the bifurcation. However, due to the subcritical nature of the instability, the Hopf modes do not saturate nonlinearly to a nearby state in phase space.

Figure 3 shows the time-series of some of the modal kinetic energies for the rotating endwalls case at $Re = 4 \times 10^5$. Shown

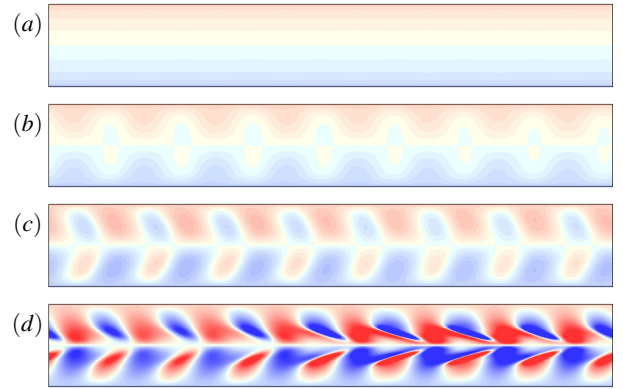


Figure 4: Azimuthal vorticity η at the inner cylinder for $Re = 4 \times 10^5$ at times (a) $t = 0.00090$, (b) $t = 0.00120$, (c) $t = 0.00130$, and (d) $t = 0.00135$. The levels are $\eta \in [-10^6, 10^6]$.

are the energies in azimuthal wavenumbers $m = 0, 1, 8$ and $8k$ for $k \in [2, 8]$ (the resolved harmonics of $m = 8$); the energies of the other wavenumbers are not shown for the sake of clarity. The time series focuses on the time when the nonlinearities are becoming important. The initial condition was the axisymmetric basic state for the same parameters, to which a small random perturbation in $m = 1$ was introduced at $t = 0$. By $t \approx 0.00028$ the first harmonic of the most dangerous Hopf mode, E_{16} , begins to grow and very shortly afterwards, E_1 also begins to grow with a marginally slower growth rate. The third harmonic, E_{24} , doesn't start to grow until $t \approx 0.00065$, and then the other higher harmonics begin to grow after shorter and shorter intervals. By $t \approx 0.0013$, all azimuthal wavenumbers (including those not harmonic with the critical m , which are not shown in the figure) begin to grow rapidly and small scale features in the boundary layer become important.

An illustration of the nonlinear development of the boundary layer flow is shown in figure 4, which shows the azimuthal vorticity, η , on the inner cylinder wall at various times for the rotating endwalls case at $Re = 4 \times 10^5$. The plots are shown at $r = r_i$ with $\theta \in [0, 2\pi]$ in the horizontal direction, and $z \in [-0.5, 0.5]$ in the vertical. At early times, $t \lesssim 0.0009$, the disturbance level is very low (from figure 3, $E_8 \lesssim 3$, compared to $E_0 \sim 10^{11}$), and the boundary layer flow is essentially axisymmetric. By $t = 0.0015$, the azimuthal wavenumber $m = 8$ component of the disturbance is large enough to have an impact on the total flow. At this stage, even though the harmonics of $m = 8$ have grown substantially, the impact of the disturbance on the wall appears essentially sinusoidal. By $t = 0.00120$, the periodic $m = 8$ structures are becoming more nonlinear, and at $t = 0.00130$ they are tilted with the structure near the mid-height being swept further in the streamwise (increasing θ) direction. At this time, the streamwise (azimuthal) vorticity structures are being aligned with the streamwise flow, resulting in vortex stretching and intensification, as seen at $t = 0.00135$. By this time, all the other azimuthal wavenumbers have also grown substantially, and their nonlinear interactions have led to a very noticeable localization in the strength of the vortex stretching and intensification. At this point, the flow is still very well resolved with $n_r = n_z = 160$ and $n_\theta = 64$. However, in a very short time later, this resolution becomes inadequate and the simulation blows up. By taking the flow at a slightly earlier time as an initial condition for a simulation with higher resolution, the simulation can be continued a little longer in time, but eventually it also blows up. Figure 5 is similar to figure 4, but for a simulation with $n_z = 1600$. Further refinements gets the simulation a little further, but one very quickly reaches the practical limit of trying to resolve this localized boundary layer



Figure 5: Azimuthal vorticity η at the inner cylinder for $Re = 4 \times 10^5$ at $t = 0.001367$. The levels are $\eta \in [-10^7, 10^7]$.



Figure 6: Azimuthal vorticity η at the outer cylinder for $Re = 4 \times 10^5$ at $t = 10^{-5}$. The levels are $\eta \in [-10^7, 10^7]$. The resolution used is $n_r = 240$, $n_z = 500$, $n_\theta = 256$ and $\delta t = 2 \times 10^{-9}$.

instability with a global spectral method.

The development of the Tollmien–Schlichting waves on the outer cylinder boundary layer when the endwalls are stationary is analogous to their development on the inner cylinder boundary layer for rotating endwalls. Figure 6 shows the azimuthal vorticity on the outer cylinder wall for $Re = 4 \times 10^5$ with stationary endwalls at a late time, just before the simulation blows up. The localized rapid growth due to the sideband modulation is more pronounced, and the counter rotating pairs of helical structures above and below the mid-height are better developed. This is in part due to the boundary layer having twice the circumference for the same azimuthal wavelength of the instability, and is also due to the simulation having better resolution.

Figure 7 shows isosurfaces of the helicity at late times for the two case discussed above. The helical structures are very flat and reside inside their respective cylinder boundary layer, whose radial thickness is only approximately 2% of the annular gap. The dark (red) isosurfaces correspond to positive He , where the velocity vector and the vorticity vector point in the same direction, and the light (yellow) isosurfaces correspond to negative He , where the two vectors point in the opposite direction. The large value of He indicates that the velocity and vorticity are well aligned. The less developed structures have negative helicity in the top half and positive helicity in the bottom half of the boundary layer. These come about because they correspond to the Tollmien–Schlichting wavelike structures being bent by the streamwise azimuthal mean flow in the boundary layer about the mid-height. The wave structures at early times correspond to azimuthally alternating positive and negative axial (spanwise) vorticity cells spanning across the entire boundary layer from top to bottom. At later times, when they are bent into the streamwise (azimuthal) direction near the mid-height, the wave structures with positive axial vorticity are bent producing negative and positive azimuthal vorticity above and below the mid-height, and vice versa for the wave structures with negative axial vorticity. The wave structures with positive axial vorticity are stronger as they are reinforced by the positive axial vorticity from the mean boundary layer flow, which in turn weakens the wave structures with negative axial vorticity. Once the wavelike structures have been bent into the azimuthal direction, they are rapidly stretched and intensified by the mean flow. The azimuthally-turned structures from the alternating wavelike structures with positive and negative axial vorticity also become intertwined. The helicity indicates that the streamwise structures consist of pairs of very closely linked counter-rotating vortices; the velocity is in the streamwise (azimuthal) direction, but one of the vortices is left-handed and the other right-handed, resulting in opposite-signed helicity. This situation rapidly leads to small-scale instability as the vortices are intensified via stretching.

Conclusions

Taylor–Couette flow with endwalls and a stationary inner cylin-

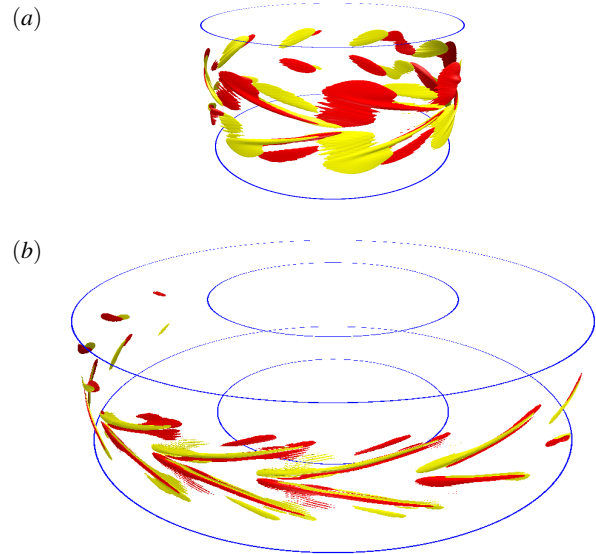


Figure 7: Isosurfaces of helicity at $Re = 4 \times 10^5$ for (a) the rotating endwalls case at $t = 0.001358$, with levels $He = \pm 7 \times 10^{10}$, and (b) the stationary endwalls case at $t = 104$, with levels $He = \pm 10^{12}$.

der is subcritically unstable. The early time form of the perturbation modes consists of rollers of alternating sign of axial vorticity that are aligned in the axial direction in the boundary layer, and behave very much like Tollmien–Schlichting waves in shear boundary layers with zero streamwise pressure gradient, where a band of waves with different wavenumbers grow leading to modulation and secondary instability. The sidewall boundary layer is very thin, implying that curvature effects are not important and accounting for the shear flow nature of the instability, initiated by vortex bending and brought to fruition by vortex stretching.

Acknowledgements

This work was supported by NSF grant CBET-1336410.

References

- [1] Avila, K. and Hof, B., High-precision Taylor–Couette experiment to study subcritical transitions and the role of boundary conditions and size effects, *Rev. Sci. Inst.*, **84**, 2013, 065106.
- [2] Burin, M. J. and Czarnocki, C. J., Subcritical transition and spiral turbulence in circular Couette flow, *J. Fluid Mech.*, **709**, 2012, 106–122.
- [3] Coles, D., Transition in circular Couette flow, *J. Fluid Mech.*, **21**, 1965, 385–425.
- [4] Lopez, J. M., Subcritical instability of finite circular couette flow with stationary inner cylinder, *J. Fluid Mech.*, **793**, 2016, 589–611.
- [5] Schmid, P. J. and Henningson, D. S., *Stability and Transition in Shear Flows*, volume 142 of *Applied Mathematical Sciences*, Springer–Verlag New York, 2001.
- [6] Taylor, G. I., Stability of a viscous liquid contained between two rotating cylinders, *Phil. Trans. Roy. Soc. Lond. A*, **223**, 1923, 289–343.